Computers and Concrete, *Vol. 21, No. 4 (2018) 367-376*
DOI: https://doi.org/10.12989/cac.2018.21.4.367

X-ray CT monitoring of macro void development in mortars exposed to sulfate attack

Ilker Tekin[1a], Recep Birgul[*2] and Huseyin Y. Aruntas[3b]

[1]*Department of Civil Engineering, Faculty of Engineering, Bayburt University, Bayburt, Turkey*
[2]*Department of Civil Engineering, Faculty of Engineering, Mugla Sitki Kocman University, Mugla, Turkey*
[3]*Department of Civil Engineering, Faculty of Technology, Gazi University, Ankara, Turkey*

(Received August 13, 2017, Revised October 12, 2017, Accepted November 22, 2017)

Abstract. This study reports the results of nondestructive monitoring of macro void developments in mortars manufactured with both ordinary Portland cement and sulfate resistant cement. Two types of curing were utilized; tap water curing and another curing environment that contains 5% $Na_2(SO_4)$ solution. Being the primary objective of this study, macro void developments of the mortar specimens were monitored by X-ray Medical Computerized Tomography. Compressive strength tests and water absorption tests were conducted on specimens that were kept in both curing environments for a duration of 560 days. Data analyses yielded consistent results among the three tests used in this experimental study. Macro void ratios of mortars decreased at the beginning of experiments for a certain period; afterwards, macro void ratios increased. The objective of this study was accomplished as anticipated since X-CT image analysis was able to nondestructively monitor macro void development process in cement mortars.

Keywords: mortar; porosity; sulfate attack; image analysis; Computerized Tomography

1. Introduction

Concrete may have to resist harsh chemicals due to environmental conditions. Either external or internal, sulfate attack is known as one of the most important mechanisms causing damage to concrete through chemical reactions. Previous studies have shown that sulfate attack may occur in various environmental conditions (Tanyildizi 2017, Mehta and Monteiro 2006). Most known sources of sulfate are sulfate ions dissolved in ground water, waste water and sea water. Sulfate ions of various concentrations penetrate into concrete through moisture from external environments and damage concrete by reacting with some compounds in cement paste.

Damages in concrete caused by sulfate attack occur in the following stages: i) formation of reaction products, ii) expansion, iii) cement-aggregate interface adhesion loss, iv) cracking and peeling, v) loss of mass and strength (Mehta and Monteiro 2006). Structures and/or structural elements such as concrete foundations of pylons, water channels, concrete conduits, pavements, dams and foundations of structures may be affected by sulfate attacks and leaching. The effects of sulfate attack are generally determined by analyzing expansion and resistance behavior of concrete. Porosity is one of the parameters that directly affects resistance and durability properties of concrete (Mehta and Monteiro 2006, Neville 1981) and can be expressed in various forms. Yaman *et al.* (2002) evaluated porosity in two groups: active porosity and passive porosity. Active void structures, also known as capillary void structures, enable penetration of aggressive ions into concrete in the form of solutions. Passive porosity was categorized as entrained and entrapped air voids. If porosity increases, compressive strength and durability decreases (Mehta and Monteiro 2006).

X-ray Computerized Tomography (X-CT) is one of the nondestructive evaluation methods. It is a convenient method to extract internal images and then analyze a material that may be composed of solid, liquid and air voids. Use of X-CT makes it possible to analyze the inner structure of concrete material by revealing information such as quantity, development and the distribution of macro void structure in the material with high level of accuracy and precision. Working principles of the X-CT system were given in previous studies (Tekin *et al.* 2010, Aruntas *et al.* 2010, Wong *et al.* 2005, Taud *et al.* 2005). The most important advantage of X-CT evaluation over other porosity measurement methods is that it can provide repetitive and nondestructively obtained internal images acquired from the very same specimens at different times (Aruntas *et al.* 2010, Martz *et al.* 1991, Martz *et al.* 1993, Morgan *et al.* 1980). While microCT is utilized to study microlevel structure of a material, X-CT is used to analyze macro structure of a material simply because one can employ much bigger experimental samples to scan. MicroCT evaluation method has also been used to determine aggregate distribution (Erdogan *et al.* 2006, Erdoğan *et al.* 2007), porosity (Tekin

∗Corresponding author, Professor
E-mail: rbirgul@gmail.com
[a]Assistant Professor
E-mail: ilkertekin@yahoo.com
[b]Professor
E-mail: aruntas@gmail.com

http://www.techno-press.org/?journal=cac&subpage=8
ISSN: 1598-8198 (Print), 1598-818X (Online)

et al. 2010, Wong and Chau 2005, Taud *et al.* 2005, Tekin *et al.* 2012) and sulfate attack effects (Stock *et al.* 2002). However, in this evaluation method, the size of the experimental specimens varies between 1 and 2.5 cm and the voids in question are micro voids. The above cited literature studied the damage mechanisms but not interested in the micro void development.

It is well known that sulfate attack causes deterioration for mortars/concretes; the main objective of the present study is not to focus on this issue. The question of this study is to examine whether or not it is possible to nondestructively monitor this deterioration process in the same experimental samples by using X-CT and substantiate the outcomes of the X-CT by the results of other tests such as water absorption and compressive tests. Therefore, in this study standard size mortars prepared with different cements were nondestructively monitored and compared in terms of macro void development of the mortars which were both exposed to sodium sulfate and water curing. Compressive strength and water absorption tests were additionally carried out to substantiate image analysis results obtained by X-CT method.

2. Materials and method

Mortar specimens were prepared by using two different cements: ordinary Portland cement (OPC) 42.5R which complies with EN 197-1,2 (2002) and sulfate resistant cement (SRC) 32.5 which complies with TS 10157 (2007). Standard CEN Sand was used in accordance with EN 196-1 (2002). The chemical and physical properties of both cement types and the standard CEN sand are presented in Table 1. Tap water was used as both mixing and curing water. Chemical analysis of water used in this study is presented in Table 2. Sodium sulfate (Na_2SO_4) in the form of powder that was used in the tests had a purity of 99.5% and it was anhydrite according to ASTM C 1012 (2002) and ASTM C452 (2002). The pH value of 1% solution obtained with this material was between 6.5 and 8.

In this experimental study, a total of 42 mortar specimens with dimensions of 40×40×160 mm were manufactured in accordance with EN 196-1 using both cement types, the details of which are presented in Table 3. The mix proportions of the mortar specimens were 0.5:1:3 water, cement and sand by weight, respectively. The specimens were kept in a laboratory environment to set and were removed from molds 24 hours later. They were cured in lime-saturated water in laboratory at 22±2℃ until they achieved a compressive strength value of 20 MPa in accordance with ASTM C1012. In the sequel, half of the mortar specimens manufactured with both cement types was placed in the curing water that contained Na2SO4 solution with a concentration of 5% and pH of 7-8 in compliance with ASTM C1012, and the remaining half of the mortar specimens were placed in tap water curing. The day when the mortars reached 20 MPa compressive strength was marked as day 0 for the experiments. On days 28, 180, 360 and 560, water absorption tests were carried out on the specimens in accordance with TS 3624 (1981). Compressive strength tests were performed on days 0, 7, 14, 21, 28, 70, 90, 120, 150, 180, 270, 360, 390 and 560. The mortar specimens were also scanned by X-CT for the purpose of macro void development analysis on the same days with compressive strength tests. Thus, the same day testing strategy enables observing the effects of macro void development on compressive strength values. Moreover, apparent porosity ratios were determined by a-water absorption tests.

Table 3 presents the experimental program of the entire study. The mortars were labeled in 3 letters. The first letter

Table 1 Chemical and physical properties of materials

Oxide (%)	OPC	SRC	Sand	Physical properties		OPC	SRC
CaO	62.40	61.77	0.21	Normal consistency (%)		28.8	25.8
SiO_2	20.27	20.10	93.59	Density (g/cm^3)		3.18	3.16
Al_2O_3	5.38	4.16	2.01	Specific surface (cm^2/g)		3262	3338
Fe_2O_3	3.42	4.85	0.43				
MgO	1.76	1.46	0.03	Fineness (%)	40 μm sieve residue	10.7	19.4
SO_3	2.77	2.50	0.08		90 μm sieve residue	0.70	2.20
K_2O	0.79	0.82	1.02	Soundness (mm)		2.0	-
Na_2O	0.02	0.08	0.60				
LOI	2.02	2.55	0.56	Initial setting time (min)		140	175
Free CaO	2.53	1.26	-				
C_3S	48.60	58.62	-	Final setting time (min)		195	275
C_3A	8.47	2.82	-				

Table 2 Chemical properties of water

Compounds	Amounts
Ca (mg/l)	28.6
Mg (mg/l)	5.4
Cl^- (mg/l)	4.4
Conductivity (µS/cm)	558-713
pH	7.0-7.6
SO_4 (mg/l)	4.8
Na (mg/l)	11.2

Table 3 Experimental program

Experiments	Test standards	Cement type	Curing type	Specimen labeling	Number of specimens	Total specimen
Compressive Str.	TS EN 196-1	OPC	Water	PWS	4	16
			Na_2SO_4	PSS	4	
		SRC	Water	SWS	4	
			Na_2SO_4	SSS	4	
X-CT	N/A	OPC	Water	PWT	2	10
			Na_2SO_4	PST	3	
		SRC	Water	SWT	2	
			Na_2SO_4	SST	3	
Water Absorption	TS 3624	OPC	Water	PWW	4	16
			Na_2SO_4	PSW	4	
		SRC	Water	SWW	4	
			Na_2SO_4	SSW	4	

Fig. 1 Mortar specimens in the X-CT scanner before the scanning operation

can be P or S; letter P, for Portland, indicates that the specimen was prepared with ordinary Portland cement, OPC cement, while the letter S, for Sulfate, indicates that the specimen was prepared with sulfate resistant cement, SRC cement. The second letter can be W or S. The letter W, for Water, indicates that the mortar specimen was cured by tap water; the letter S, again for Sulfate, indicates that the mortar specimen was cured with sulfate solution cure. The third and last letter indicates which specimen was subject to what test. The letter W indicates Water absorption tests, the letter S indicates compressive Strength tests and the letter T shows X-CT tests.

2.1 Monitoring of the development of macro voids by X-CT

As seen in Fig. 1 General Electric (GE) Light speed scan VCTi model medical X-CT having a third generation matrix detector was used for monitoring the development of macro voids in mortars. Settings of the X-CT on each scanning day were as follows: axial scanning mode, 120 kV peak of energy level, 400 mA X-ray tube current, 0.625 mm slice thickness, 0.1875×0.1875 pixel size and 512×512 pixel matrix. Each image obtained by this technique was stored in Digital Imaging and Communications in Medicine (DICOM) format. A total of 256 images were attained from each X-CT scanning operation that was performed on each mortar specimen with a length of 160 mm. Each of these X-CT data sets covers 0.625 mm×256=160 mm of each samples' length. Among 256 X-CT images obtained from each specimen, the first and the last 3 images were not included in analyses due to the defects on the images. This issue was previously reported by Birgul (2008). All X-CT images were obtained by keeping the X-CT settings constant. These images were analyzed using a software program prepared in MATLAB v.10a; void ratios of each specimen were separately determined.

Data analyses were carried out as follows: X-CT images in DICOM format were first entered into the Matlab workspace and then each image was reconstructed in Matlab environment as shown in the center of Fig. 2. Then, border lines were drawn 5 mm from the outer edges of mortar specimens to specify the region of interest. Development analysis of macro void structure was performed within this bordered area. The reason for analyzing the inner section was to minimize "Beam Hardening" error, which was one of the errors caused by X-rays of CT. The image in the center of Fig. 2 shows the raw data and the area determined as the region of interest; raw data obtained from the material in this bordered area is presented in left upper corner. The other images are black and white images obtained afterwards according to different threshold values of the same bordered area.

In Fig. 2, the side images are the images of the area that is bordered by dash-dot lines on the image shown in the center. On these images, white areas depict solid sections, black areas depict voids. Before constructing these images, a threshold Hounsfield Unit (HU) value had been obtained to determine the transition value from the solid parts to the void parts of the mortar. Separate statistical analyses were

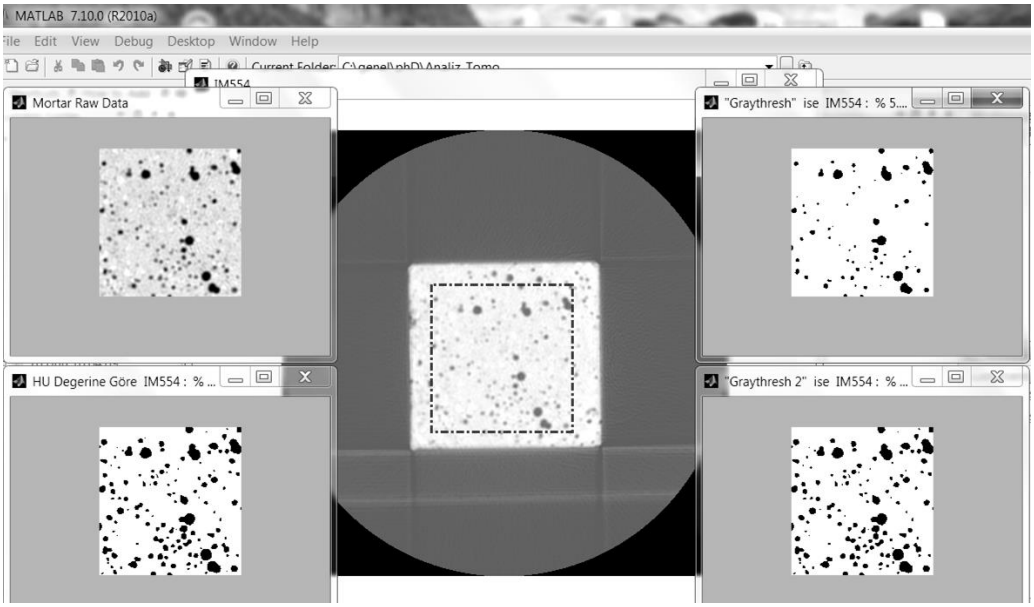

Fig. 2 A raw X-CT image and the effects of different threshold values on the image

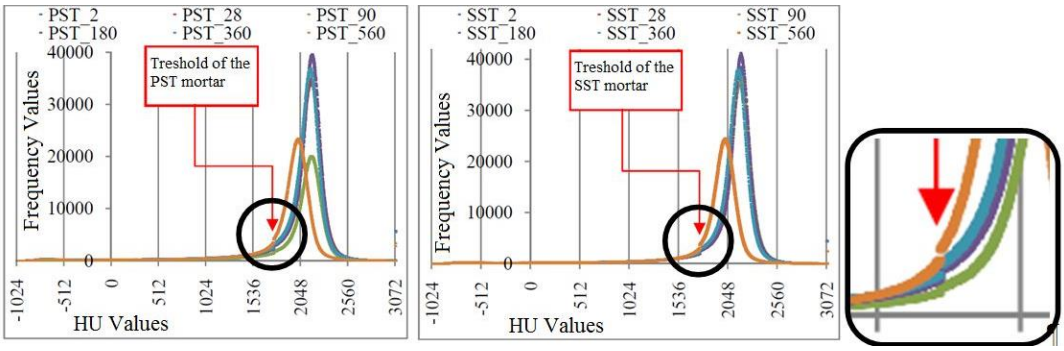

Fig. 3 Determination of the threshold HU value by frequency analysis

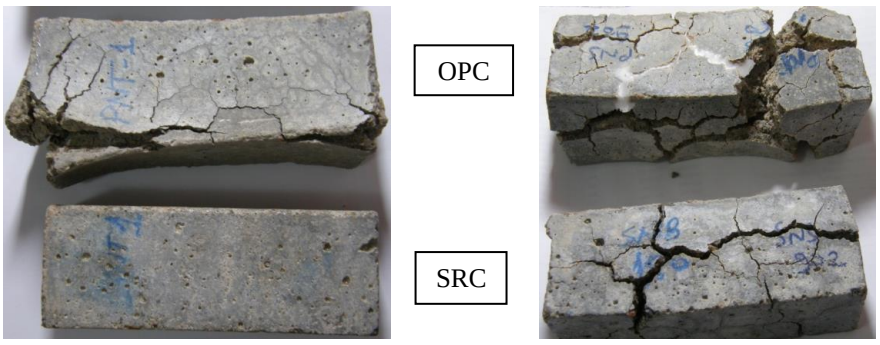

(a) X-CT scanned specimens (b) Exposed to water absorption tests

Fig. 4 OPC and SRC mortar specimens exposed to Na2SO4 solution at 560 days of age

Table 4 Apparent porosity measurements by water absorption tests

Mortar type	Descriptive statistics	n	Age (Day)			
			28	180	360	560
PWW	μ	4	13.58	13.52	13.64	14.16
	σ		0.34	0.38	0.46	0.55
PSW	μ	4	12.38	12.48	12.87	19.44
	σ		0.21	0.43	0.88	0.61
SWW	μ	4	14.95	14.96	15.1	16.02
	σ		0.15	0.06	0.26	0.53
SSW	μ	4	13.22	13.28	13.7	16.56
	σ		0.35	0.57	0.43	0.94

made in Microsoft Office Excel and Matlab. First, HU values in the images obtained from X-CT scans were transferred to Microsoft Office Excel and all HU values in each specimen were placed in a frequency curve. The obtained curve formed the Gauss curve. After determining 95% confidence interval on this curve, upper and lower limits for HU values of mortar specimens were defined. However, a discontinuity as indicated in Fig. 3 was observed in all frequency curves. The sections in circles in Fig. 3 were magnified and presented next to the figure. This point indicated very close HU values in frequency curves of all mortar specimens. Threshold HU values were found to be 1740 - 1760 HU using MS Excel. Later, a threshold HU value by using graythresh function of Matlab software was found to be 1748 HU. The authors decided to use the threshold value of 1750 HU following the results of frequency analyses. After defining threshold value as 1750, the bottom image on the right side in Fig. 2 was obtained by using the program prepared in Matlab V.10a. The areas formed by pixel values below threshold value (macro voids) were indicated in black; the areas formed by pixel values above threshold value (solid parts of mortar) were indicated in white. The void ratio for a scanned image was obtained by dividing the areas formed by black parts into the entire image area. This process was applied to all the images gathered from a specimen. Then, the average of all void ratios was taken to determine the void ratio of the specimen.

3. Results and discussion

3.1 Water absorption test results

Apparent void ratio measurement results obtained from water absorption tests are presented in Table 4. As seen in this table, both dry specific gravity and apparent void ratio results generally increased in mortars exposed to $Na_2(SO_4)$ for a period of 560 days. While dry specific gravity values of water cured mortars increased with age, apparent void ratio values of the same mortars decreased up to 180th day but increased after the 180th day. When compared to the results of 28th day tests, apparent void ratios of mortars manufactured with OPC and SRC that were in water cure during 560-day duration increased by 0.58% and 1.07% respectively. On the other hand, when compared to the results of 28th day, apparent void ratio values of OPC and SRC mortars exposed to sodium sulfate increased by 7.06% and 3.34% respectively.

Final conditions of the mortars at 560th day are presented in Fig. 4. The images on the top side show OPC

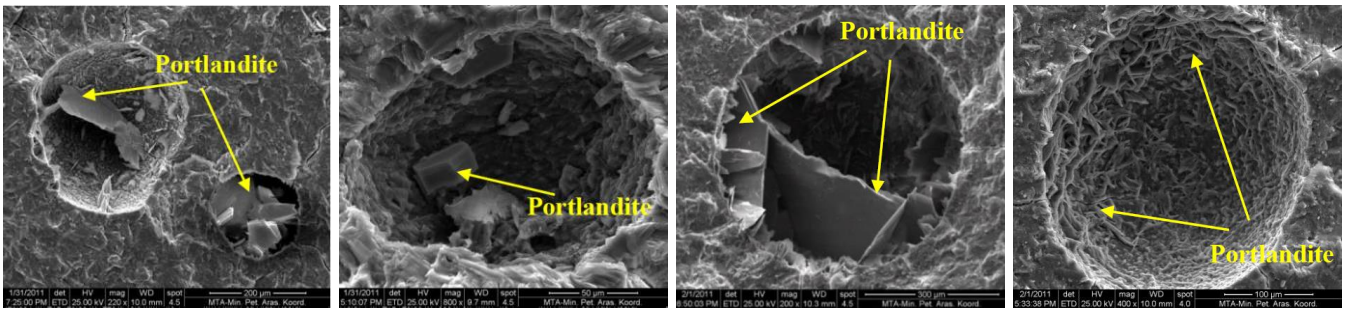

(a) PWT (b) PST (c) SWT (d) SST

Fig. 5 SEM images of mortars at the age of 360 day

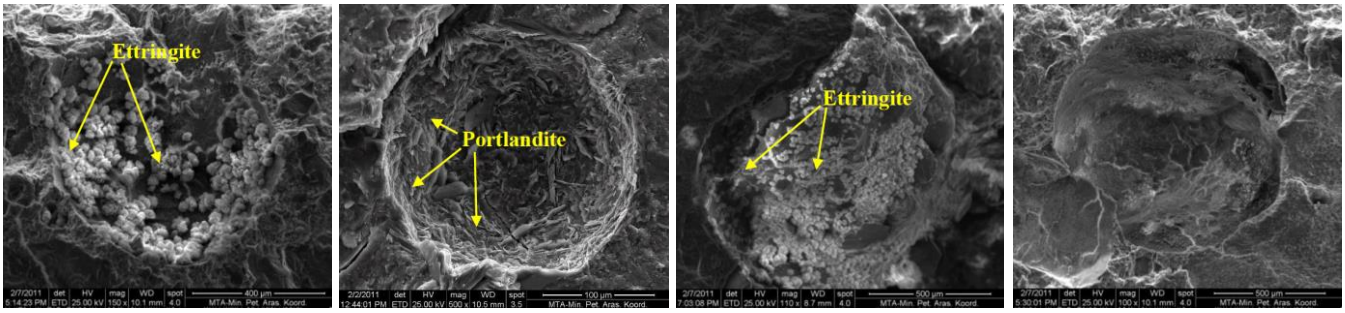

(a) PWT (b) PNT (c) SWT (d) SST

Fig. 6 SEM images of mortars at the age of 560 day

mortar specimens and the images on the bottom side show SRC mortar specimens. The mortars subjected to X-CT scans on testing days during 560-day period are presented in Fig. 4(a), the mortars subjected to water absorption tests are presented in Fig. 4(b). The fact that water absorption tests were repeated for 4 times caused the mortar specimens that were exposed to sulfate attack undergo more deterioration. As known, repetitive soaking-drying cycles accelerate damage mechanisms of sulfate attack (Mehta and Monteiro 2006).

The process known as leaching (Mehta and Monteiro 2006) was the reason for the increase in apparent void ratios of the same mortar specimens that were exposed to four cycles of water absorption tests for 560-day duration; the specimens underwent repetitive cycles of wetting and drying. In this process, water in both curing types where the mortars were placed was renewed approximately in every 30 days leading to a decrease in pH value of the curing water. Thus, crystal structures in some pores were washed away and dissolved into curing water, and in turn, apparent void ratios increased. As shown in SEM images given in Fig. 5 and Fig. 6, this process was more clearly observed in macro voids having diameter sizes greater than 200 μm. Fig. 6 depicts that the pores have small amounts of portlandite and ettringite crystals at the end of 560-day duration.

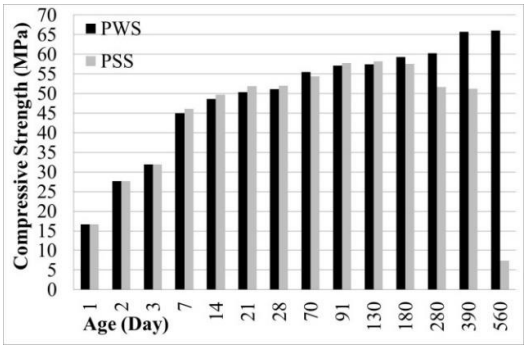

(a) OPC mortars

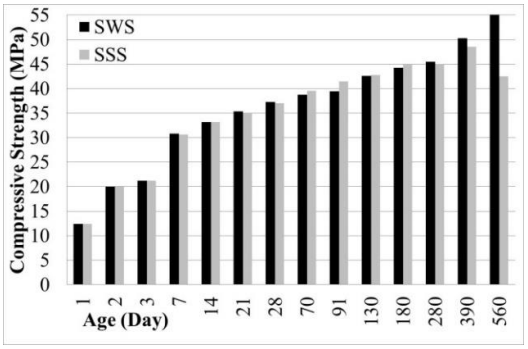

(b) SRC mortars

Fig. 7 Compressive strength development with age

3.2 Results of compressive strength tests

Presented in Fig. 7 is compressive strength developments of OPC and SRC mortars. It can be seen from Fig. 7(a) that the average compressive strength values of PSS were lower than that of PWS mortars after 130th day. Similarly, Fig. 7(b) shows that the average compressive strength values of SSS mortars were lower than that of SWS after 180th day. It is known that Na_2SO_4 effect increases compressive strength of mortars/concretes until a certain age (Mehta and Monteiro 2006). This increase in compressive strength value was explained by the increase of solid concentration

of the material that was caused by reaction products filling the micro and macro pores in mortars/concretes. The decrease that occurred later in compressive strengths was explained by the fact that sulfate reacted with portlandite inside the pores and formed expansion products such as gypsum and ettringite (Zuo *et al.* 2012).

3.3 Analysis of macro void ratios by X- CT method

Macro void development ratio information given below is obtained from the image analyses of X-CT images as explained in Section 2.2.1, Fig. 8 depicts the results of these analyses. It is observed from the figure that the trends of macro void developments are similar in both types of cements. However, in 560-day duration, more deterioration occurred in OPC mortars when compared to SRC mortars due to lower C_3A ratio in SRC. As shown in Fig. 8, the average values of macro void ratios of PWT and SWT mortars decreased up to 120th day by 1.2% and 1.1%, respectively, and increased between the days 120 and 560 by 4.1 % and 3.5%, respectively. On the other hand, the decrease in macro void ratios for PST and SST mortars continued up to 270th day; the amounts of decrease calculated on that day were 0.7% and 0.8%, respectively. The void ratios for PST and SST mortars increased between the days 270 and 560 by the amounts of 8.8% and 5.1%, respectively. At the end of 560-day duration, when compared to the first measurement day, the void ratios of PST mortars increased approximately 1.6 times whereas the void ratios of SST mortars increased by approximately 1.3 times. The increase in macro void ratios observed from X-CT image analysis results from the dropped alkalinity in curing water due to periodical water renewal. pH values that varied after the renewal of curing water are presented in Table 5. It is known that sulfate effect depends on pH value and sulfate attack damage increases when the pH value of the sulfate solution is between 6 to 8 (Xiong *et al.* 2015). Both sulfate solution and curing water were renewed every 30-days since pH values reached to a maximum approximately in 30 days; thus pH values of the curing water brought back to approximately 7 after each renewal.

The decrease in macro void ratios of OPC and SRC mortars was explained as follows: portlandite crystals that precipitated in the pores of the mortars increased density, thus HU values of the areas in X-CT images increased as well since the density of these areas in the mortars increased. The values above a certain threshold value, as explained in Section 2.2.1, give indications to solid parts while the values below this threshold value denote macro voids. Therefore, the rise in HU values corresponds to the decrease in void ratios. The increase in macro void ratio in later ages can be explained as follows: periodically renewed curing water washed away such hydration products as portlandite in the pores, and in turn, the density in the pores decreased, leading to lower HU values for these regions in the X-CT images. The fall in HU values corresponds to the increase in void ratios. Descriptive statistics of the development of density values in mortar specimens in terms of HU values obtained from X-CT images are presented in Table 6. This table shows that HU values that increased up to 180th day decreased in later ages due to increased void ratios in the mortars.

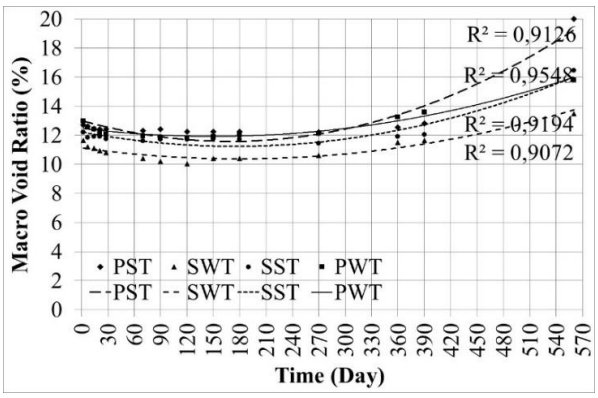

Fig. 8 Development of macro voids by X-CT tests

Table 5 Variations in pH values of curing water

Age (Day)	Water (1st measure)	Water (last measure)	$Na_2(SO_4)$ (1st measure)	$Na_2(SO_4)$ (last measure)
1 - 7	7.0	11.5	9.0	11.0
7 - 14	7.4	12.0	7.8	10.0
14 - 28	7.2	9.8	7.6	11.3
28 - 70	7.1	11.0	7.5	11.2
70 - 180	7.2	10.5	7.6	10.8
180 - 200	7.2	12.2	7.7	12.4
330 - 360	7.3	9.6	7.3	12.1
360 - 420	7.1	9.0	7.5	10.5
420 - 480	7.2	9.0	7.5	9.8
480 - 560	7.2	9.2	7.5	10.5

Table 6 HU values of mortars with respect to time

No	Statistics	Curing age (Day)						
		2	7	28	90	180	360	560
PWT	μ	2001	2012	2016	2024	2025	1983	1876
	σ	24.87	24.71	23.84	22.48	21.62	24.02	21.84
	Error	1.56	1.55	1.50	1.63	1.57	1.72	2.13
PST	μ	2014	2021	2018	2018	2027	2017	1872
	σ	25.46	24.74	24.70	21.95	21.91	22.53	22.84
	Error	1.60	1.55	1.55	1.59	1.58	1.65	2.16
SWT	μ	2025	2036	2037	2051	2050	2004	1890
	σ	25.27	23.53	22.77	19.67	20.41	23.36	19.92
	Error	1.59	1.48	1.43	1.39	1.44	1.64	1.82
SST	μ	2026	2034	2030	2030	2040	2028	1892
	σ	28.15	26.80	26.83	26.01	24.91	25.56	23.05
	Error	1.77	1.69	1.69	1.82	1.75	1.80	2.11

Tekin *et al*. (2012) reported that the decrease in macro void volume of OPC mortars continues for a period of 100 days. In cementitious systems, curing water with low pH value washes away hydration products and consequently hydrates of cement paste become hydrolyzed. The pH of void solution decreases when the dissolved products are transferred to curing water. Primary dissolved hydrate is $Ca(OH)_2$. Dissolution of portlandite is closely related with increased capillary porosity. A high ratio of porosity increase is the main result of this dissolution (Burlion *et al.*

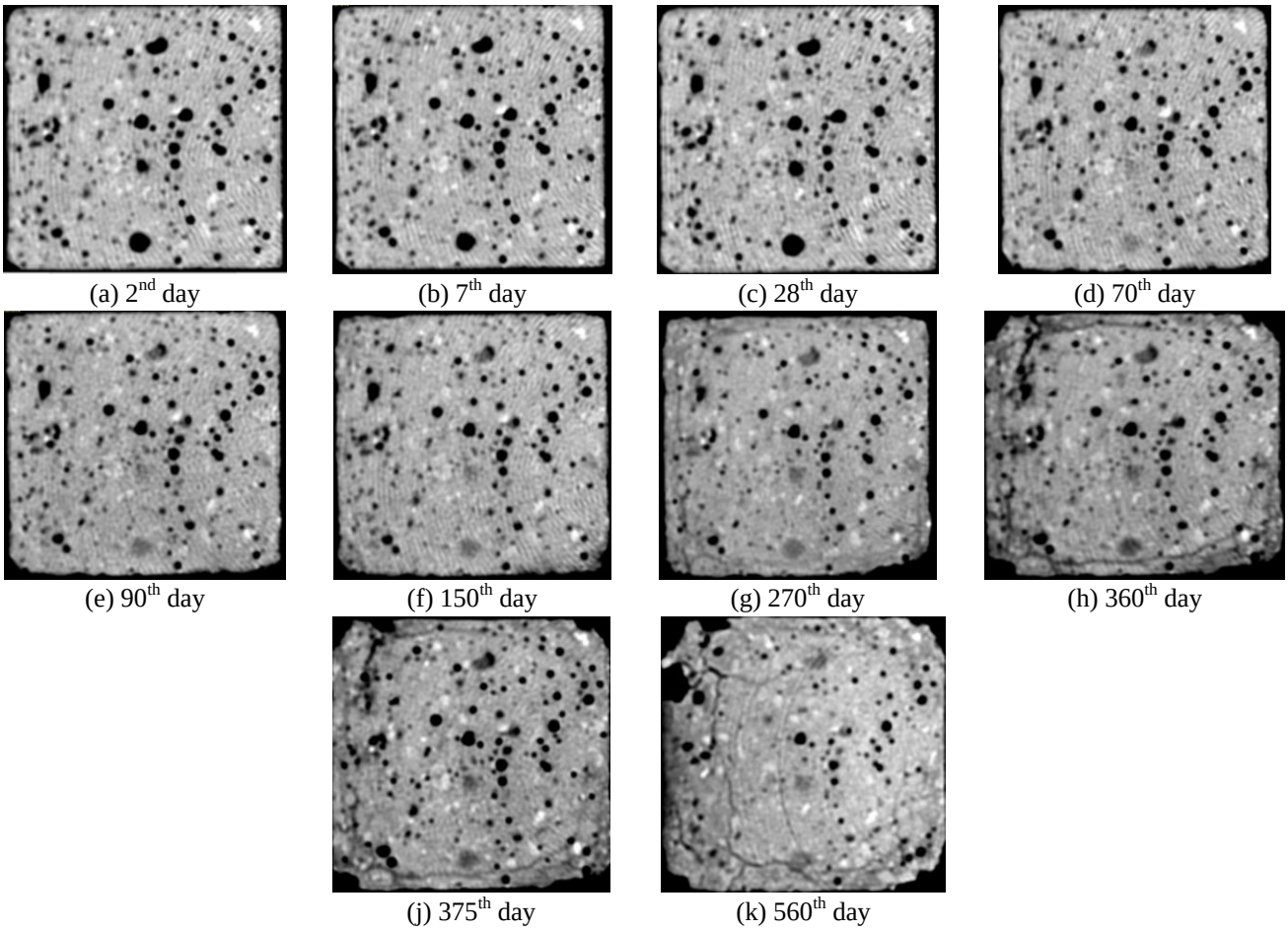

Fig. 9 The X-CT images of an OPC mortar on different days for the same slice (10th X-CT slice)

2006).

No crack was observed in SRC mortars during the course of this study. However, deterioration in OPC mortars that were exposed to sulfate during the same period was clearly observed. The development of this deterioration inside the mortar is monitored by extracting X-CT images from an OPC mortar on different days for the same slice and is presented in Fig. 9. This figure shows that cracks caused by sulfate effect increased the porosity in the specimen. Firstly, reaction products were formed because of sulfate effect; secondly, the voids were filled by these products (Fig. 9(d) through (k)); and lastly, adhesion strength decreased due to distorted pH balance (Fig. 9(g) through (k)). It was reported in the literature that in mortars exposed to sulfate effect, pore volume decreased for a certain period and increased later (Xiong *et al.* 2015, Yin *et al.* 2017, Zuo *et al.* 2017). It is shown in Fig. 9 that some voids on day 2 that are indicated in black color turned to gray color after day 70, meaning that the density of these regions increased. This led to the increase of HU values of these regions which were previously registered as macro voids and consequently the area of voids decreased.

Increased density of some voids in Fig. 9 is an indication of crystallization caused by the formation of reaction products. It was observed that damage behavior of the specimens that were exposed to Na_2SO_4 in Fig. 9 was consistent with the model developed by Santhanam *et al.* (2003). It is also observed from Fig. 9 that material loss took place on surfaces of the mortar specimen in the form of peelings; then the cracks propagated towards inner parts of the specimen. In addition, damage start was observed on the sides of this specimen after 70th day. Analyses on the images of this specimen conducted on the 270th day revealed that crack lines started approximately 5 mm inside the edge of the specimen. The cracks on this specimen were clearly visible in the first 10 and in the last 30 X-CT images (the first 6 mm and the last 20 mm of the specimen); but these images were not included in order not to congest the paper. Analysis results of macro void ratios of the mortars that were exposed to $Na_2(SO_4)$ solution are presented in Fig. 10(a) and Fig. 10(b); X-CT images to analyze were taken on 14th and 560th days of the study.

Analysis results of macro void ratios of tap water cured mortar specimens on 2nd and 560th days are presented in Fig. 10(c) and Fig. 10(d). A total of 251 cross-sections were scanned on both days from the mortars exposed to sulfate. Each X-CT image produced a macro void ratio value. The void ratio results are presented in Fig. 10(a) and Fig. 10(b) in the form of X-CT slices vs macro void ratio percentages. As for the tap water cured mortars, Fig. 10(c) and Fig. 10(d) are missing some information regarding the 560th day X-CT scan analysis results since the last 40 mm sections of both specimens were cut to perform compressive strength tests on the tap water cured mortar specimens; thus, no image

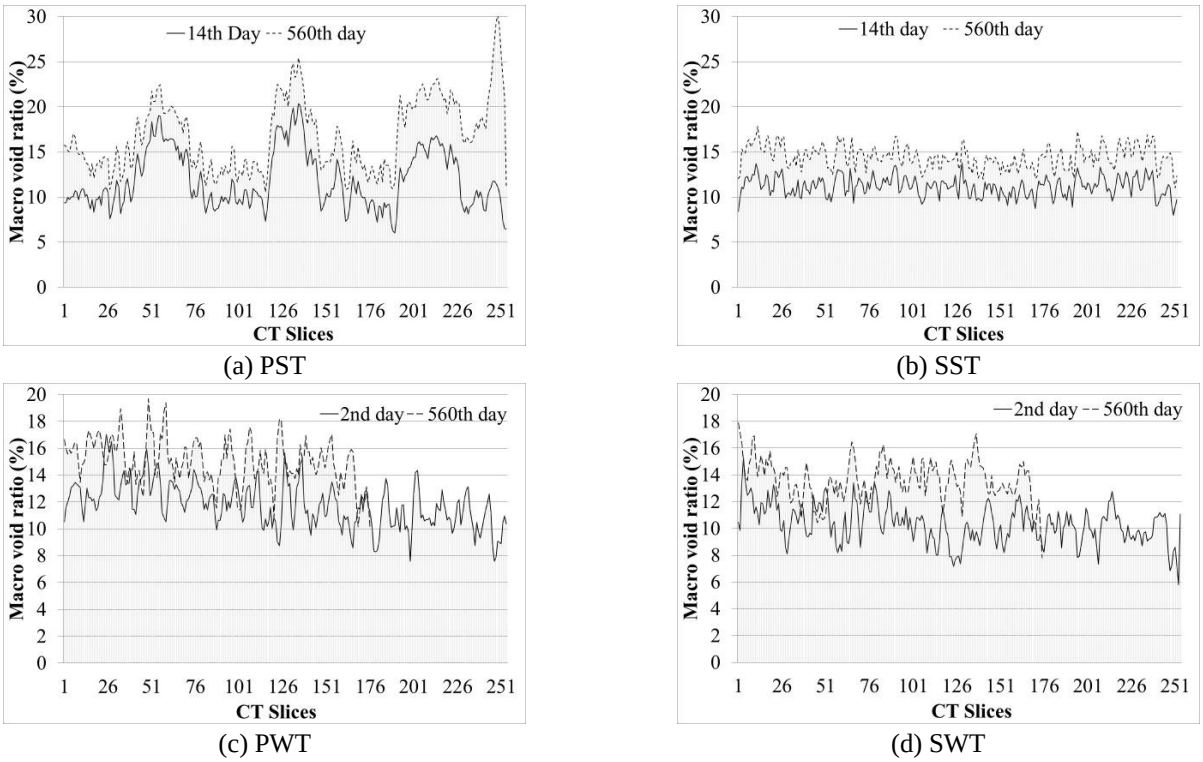

Fig. 10 Macro void distributions of mortars by X-CT analyses

could be taken from that part of the specimens on the 560th day. Therefore, image analyses on 560th day were performed only on remaining 160 images. Close examination of Fig. 10 indicates that macro void ratios clearly increased for every cross-section in all mortars. As can also be seen from Fig. 10 that, on the 2nd and 14th days of X-CT tests, void ratios were between 7 and 20% in OPC mortars and were between 6 and 15% in SRC mortars.

According to the analysis results, void ratios of the specimens that were exposed to sulfate gave close values in X-CT measurements and water absorption measurements during the course of this study. Apparent porosity ratios obtained by water absorption tests for a duration of 560 days were 0.6%, 1.1%, 7.1%, 3.3% for PWW, SWW, PSW and SSW mortars; on the other hand, macro void ratios obtained by X-CT image analyses were 2.9%, 2.4%, 8.1% and 4.3% for PWT, SWT, PST and SST mortars. Porosity information obtained by both techniques yielded similar results although all porosity values obtained by water absorption tests were consistently a little lower than those of X-CT image analyses. It was speculated that the reason for lower porosity values of water absorption tests was the intrinsic difficulty to fill the voids of the mortars by the absorbed water.

Total macro void ratio results of OPC mortars rapidly decreased between the days 2 and 28, while their strengths rapidly increased according to the results of X-CT analysis. After that, almost a horizontal trend of compressive strengths and macro void ratios of PSS and PST mortars between the days 28 and 360 were observed. Macro void ratios showed a rapid increase while compressive strengths showed a rapid decrease between the days 360 and 560 according to the test results of X-CT analysis. It can be stated that macro void development ratio values and compressive strength values of OPC mortar specimens that were exposed to sulfate are reversely proportional. Similarly, a decrease in macro void ratios between the days 2 and 180 was observed as compressive strength increased during the same period for SRC specimens. After 180th day, macro void ratios rapidly increased and compressive strength values decreased for especially SSS mortar specimens.

4. Conclusions

The following conclusions can be drawn from this study:

- The threshold value to distinguish voids from solids for OPC and SRC mortar specimens were found to be between 1740 and 1760 HU. The pixels showing values below this range of HU values denote voids while the values above this range indicate solid sections of the mortars.
- If any changes are made to the composition of materials used to manufacture experimental specimens in general, a threshold value to differentiate the transition from solid state to void state must be determined first before proceeding with any X-CT image analysis.
- X-CT image analysis can effectively be utilized as a nondestructive tool to continuously monitor the macro void developments in the very same experimental specimens throughout the monitoring period. Unless used for compressive strength tests, the same specimens can be repeatedly subject to the same tests on different

days in an experimental study. In this fashion, macro void development monitoring will be more informative and reliable for mortars/concretes.

• X-CT analyses showed that macro void ratios of all mortars decreased between the days 2 and 180. However, they increased in varying ratios in all mortars between the days 180 and 560. Macro void ratios showed an average increase of 1.6 times in the specimens that were exposed to sulfate and an average increase of 1.3 times in tap water cured specimens. This results are in good agreement with the results of apparent porosity values of PSS and SSS mortar specimens.

• The average HU values of the specimens obtained on the 2nd day decreased to a lower average HU values on 560th day for all mortars. This result of X-CT image analysis is an indication of increased deterioration in the mortar specimens.

• Compressive strength values of the mortars under sulfate effect decreased after 130th day in OPC and after 180th day in SRC. The results of compressive strength tests are in good agreement with the increase in macro void ratios on the same days monitored by X-CT image analyses.

Acknowledgments

This study was supported by TUBITAK Project no 109M727. Furthermore, Turkish Cement Manufacturers' Association provided financial support for the study within the framework of "Izbırakanlar" Scholarship. The authors would like to thank to SODAŞ A.Ş. Denizli Çardak Manufacturing plant for supplying the sodium sulfate used in this study; to the management of LİMAK Ankara Güvercinlik Cement Factory for the supply of both types of cements; Assoc. Prof. Dr. Gonca Erbaş and technician Seyhan Erdem at Gazi University Faculty of Medicine Department of Radiology for their contribution in obtaining the tomography images.

References

Aruntas, H.Y., Tekin, I. and Birgül, R. (2010), "Determining Hounsfield Unit values of mortar constituents by computerized tomography", *Measure.*, **43**(3), 410-414.

ASTM C 1012 (2002), Standard Test Method for Length Change of Hydraulic-Cement Mortars Exposed to a Sulfate Solution, Annual Book of ASTM Standards, USA.

ASTM C452 (2002), Standard Test Method for Potential Expansion of Portland-Cement Mortars Exposed to Sulfate, Annual Book of ASTM Standards, USA.

Birgul, R. (2008), "Monitoring macro voids in mortar by X-ray computed tomography", *Nucl. Instr. Meth. Phys. Res. A*, **596**, 459-66.

Burlion, N., Bernard, D. and Chena, D. (2006), "X-ray microtomography: Application to microstructure analysis of a cementitious material during leaching process", *Cement Concrete Res.*, **36**(2), 346-357.

Erdoğan, S.T., Garboczi, E.J. and Fowler, D.W. (2007), "Shape and size of microfine aggregates: X-ray microcomputed tomography vs. laser diffraction", *Powder. Technol*., **177**(2), 53-63.

Erdogan, S.T., Quiroga, P.N., Fowler, D.W., Saleh, H.A., Livingston, R.A., Garboczi, E.J., Ketcham, P.M., Hagedorn, J.G. and Satterfield, S.G. (2006), "Three-dimensional shape analysis of coarse aggregates: New techniques for and preliminary results on several different coarse aggregates and reference rocks", *Cement Concrete Res.*, **36**(9), 1619-1627.

Martz, H.E., Roberson, G.P., Skeate, M.F., Schneberk, D.J. and Azevedo, S.G. (1991), "Computerized tomography analysis of reinforced concrete", *Mater. J.*, **90**(3), 259-264.

Martz, H.E., Scheberk, D.J., Roberson, G.P. and Monteiro, P.J.M. (1993), "Computerized Tomography Analysis of Reinforced Concrete", *Mater. J. Am. Concrete Inst.*, **90**(3), 259-264.

Mehta, P.K. and Monteiro, P.J.M. (2006), *Concrete: Microstructure, Properties and Materials*, 2nd Edition, McGraw Hill, New York, USA.

Morgan, I.L., Ellinger, H., Klinksiek, R. and Thompson, J.N. (1980), "Examination of concrete by computerized tomography", *ACI J. Proc.*, **77**(1), 23-27.

Naik, N.N., Jupe, A.C., Stock, S.R., Wilkinson, A.P., Leed, P.L. and Kurtis, K.E. (2006), "Sulfate attack monitored by microCT and EDXRD: Influence of cement type, water-to-cement ratio, and aggregate", *Cement Concrete Res.*, **36**(1), 144-159.

Neville, A.M. (1981), *Properties of Concrete*, 3rd Edition, Longman Scientific & Technical, England.

Santhanam, M., Cohen, M.D. and Olek, J., (2003), "Mechanism of sulfate attack: A fresh look: Part 2: Proposed mechanisms", *Cement Concrete Res.*, **33**(3), 341-346.

Stock, S.R., Naik, N.K., Wilkinson, A.P. and Kurtis, K.E. (2002), "X-ray micro tomography (microCT) of the progression of sulfate attack of cement paste", *Cement Concrete Res.*, **32**(10), 1673-1675.

Tanyildizi, H. (2017), "Prediction of compressive strength of lightweight mortar exposed to sulfate attack", *Comput. Concrete*, **19**(2), 217-226.

Taud, H., Martinez-Angeles, R., Parrot, J.F. and Hernandez-Escobedo, L. (2005), "Porosity estimation method by X-ray computed tomography", *J. Petrol Sci. Eng.*, **47**(3-4), 209-217.

Tekin, I., Birgül, R. and Aruntaş, H.Y. (2010), "Determination of void development in cement mortar by computerized tomography", *Cement Concrete World*, **13**, 67-76.

Tekin, I., Birgul, R. and Aruntas, H.Y. (2012), "Determination of the effect of volcanic pumice replacement on macro void development for blended cement mortars by computerized tomography", *Concrete Build. Mater.*, **35**, 15-22.

TS 10157 (2007), Cement-Composition, Specifications and Conformity Criteria for Sulphate-Resisting Cement, Institute of Turkish Standards, Ankara, Turkey.

TS 3624 (1981), Test Method for Determination the Specific Gravity the Absorption Water and the Void Ratio in Hardened Concrete, Institute of Turkish Standards, Ankara, Turkey.

TS EN 196-1 (2002), Methods of Testing Cement-Part 1: Determination of Strength, Institute of Turkish Standards, Ankara, Turkey.

TS EN 197-1 (2002), Cement-Part 1: Composition, Specifications and Conformity Criteria for Common Cements, Institute of Turkish Standards, Ankara, Turkey.

TS EN 197-2 (2002), Cement-Part 2: Conformity Evaluation, Institute of Turkish Standards, Ankara, Turkey.

Wong, R.C.K. and Chau, K.T. (2005), "Estimation of air void and aggregate spatial distributions in concrete under uniaxial compression using computer tomography scanning", *Cement Concrete Res.*, **35**(8), 1566-1576.

Xiong, C., Jiang, L., Zhang, Y. and Chu, H. (2015), "Modeling of damage in cement paste subject to external sulfate attack", *Comput. Concrete*, **16**(6), 847-864.

Yaman, I.O., Hearn, N. and Aktan, H.M. (2002), "Active and non-active porosity in concrete Part I: Experimental evidence", *Mater. Struct.*, **35**, 102-109.
Yaman, I.O., Hearn, N. and Aktan, H.M. (2002), "Active and non-active porosity in concrete Part II: Evaluation of existing models", *Mater. Struct.*, **35**, 110-116.
Yin, G., Zuo, X, Tang, Y., Ayinde, O. and Ding, D. (2017), "Modeling of time-varying stress in concrete under axial loading and sulfate attack", *Comput. Concrete*, **19**(2), 143-152.
Zuo, X., Sun, W., Li, H. and Zhao, Y. (2012), "Modeling of diffusion-reaction behavior of sulfate ion in concrete under sulfate environments", *Comput. Concrete*, **10**(1), 79-93.
Zuo, X., Wang, J., Sun, W., Li, H. and Yin, G., (2017), "Numerical investigation on gypsum and ettringite formation in cement pastes subjected to sulfate attack", *Comput. Concrete*, **19**(1), 19-31.

CC